Absorption measurement of layers or materials: How to calibrate?

Hervé Piombini, Amira Guediche, Didier Picart, Gilles Dammame

ABSORPTION MEASUREMENT OF LAYERS OR MATERIALS: HOW TO CALIBRATE?

H. PIOMBINI,[1*] AMIRA GUEDICHE[1],D. PICART,[1] AND G. DAMMAME[2]

[1]*CEA, DAM Le Ripault, F-37260 Monts, France*
[2]*CEA, DAM Centre de Gramat F-46500 Gramat France*
**herve.piombini@cea.fr*

Abstract: The knowledge of the absorption in the optical materials is important because it can generate problematic phenomena (distortion, depolarization, damage...) when high-power lasers are used. **P**hotothermal **D**eflection (P.D.) makes it possible to quantify it with the measurement of the deflection of a probe beam caused by the propagation of a pump laser in the material or a thin layer. The deflection depends on the thermomechanical parameters and needs to be calibrated. The purpose of this paper is to present a method for measuring the absorption and to establish simple ratios to estimate it. This method is supported with a thermal modeling.

1. Introduction

The absorption denoted A in the optical material limits their use in the laser field, especially for high-power laser. The absorption is divided into two terms: one for the scattering denoted A_S and the other for thermal absorption denoted A_T. If the first matches the spray of the light, the second generates heat when optical components are irradiated with high-power lasers. This temperature rise induces distortions [1-3] of wavefront, self-focusing [4-5], depolarization [6-7], laser damage [8] and modifications of electronic transport properties [9-10] . The high-power laser channels require dioptric systems made of highly transparent materials such as silica and high quality coatings in order to avoid the effects of the thermal absorption. The excellent transparency of silica is well known for its various applications in the field of optical fibers. An example of optical losses in fibers as a function of the wavelength is drawn in **Fig 1** [11].

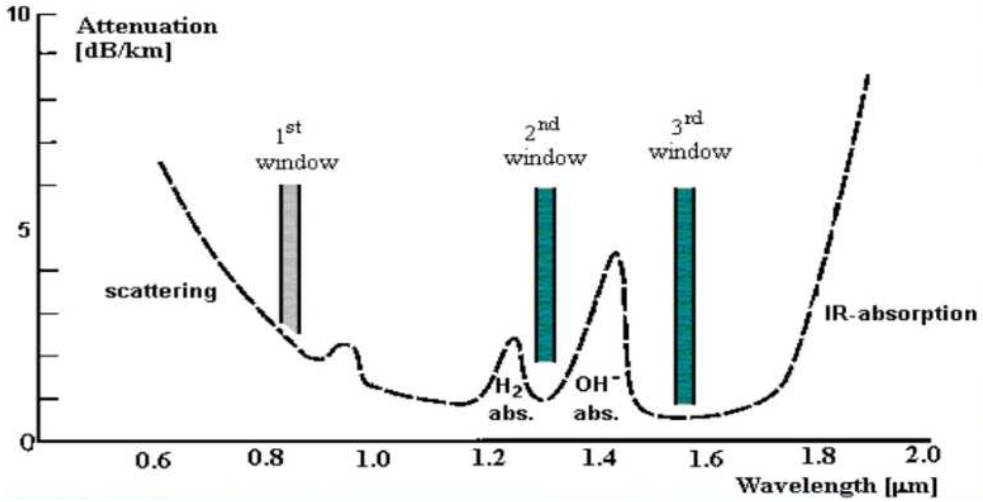

Fig. 1: Losses in dB·km^{-1} as a function of the wavelength for a silica fiber from [11].

Bentham Company supplied the attenuation spectra of their optical fibers (FOP) in the spectral range of [200-2200 nm].These fibers contain lots hydroxyl groups (OH^-) [12], which are detectable with absorption peaks at 725, 880, 950, 1230 and 1370 nm [13].

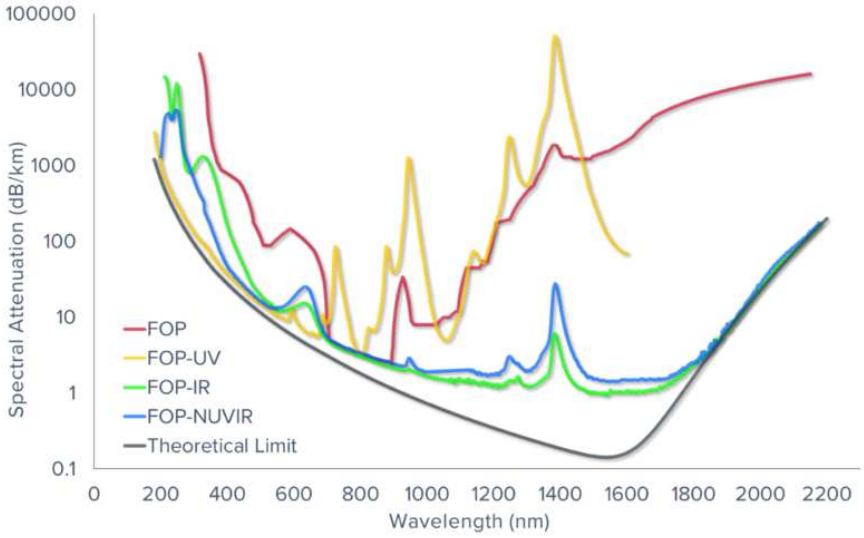

Fig. 2: Losses in $dB \cdot km^{-1}$ as a function of the wavelength in ultraviolet (UV), visible and infrared (IR) range for optical fibers in borosilicate glass (FOP), in pure fused silica (FOP-UV and FOP-IR) and in low hydroxyl pure fused silica (FOP-NUVIR) and the theoretical limit [10].

The concentration of OH^- free ions plays an important role in silica absorption; the higher the concentration, the higher the absorption is [12].

Figure 3 gives the intrinsic absorption of different silica materials produced by Heraeus Company. These values are taken at 350 and 510 nm [13].

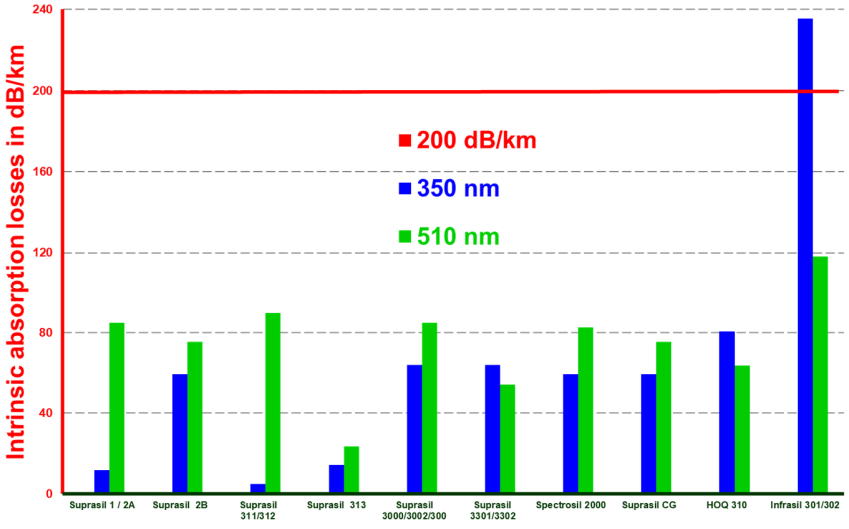

Fig. 3: Bar graph of intrinsic absorption losses in $dB \cdot km^{-1}$ at 350 and 510 nm calculated from spectra given by Heraeus Company [15].

This bar graph clearly illustrates how is difficult to measure the silica absorption. Most of the values are lower than 200 $dB \cdot km^{-1}$ (see **Fig.3**). Sometimes some absorption values at 350 nm are lower than those at 510 nm.
The main problem is the use of spectrophotometers to make these measurements but their accuracy is limited to 1000 to 2000 ppm [16]. The absorption of weakly absorbent materials such as BK7 can be estimated from a measurement carried out by spectrophotometry with two samples: one thin and the other thick (see **Fig 4**). The method of cavity ring-down spectroscopy [17-18] can also be a solution, but to avoid a fit with several samples having different thicknesses [19], both faces of the sample must be polished at Brewster's angle. However for silica, the sensitivity of these devices is not high enough and another method, such as the photothermal method, must be used [20-31].

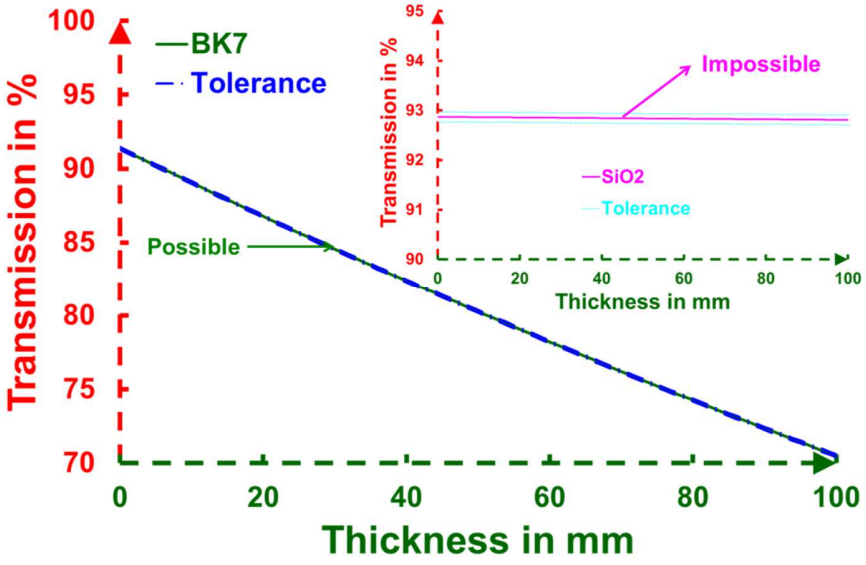

Fig. 4: Calculated transmission as a function of the thickness for BK7 and silica samples using internet data [30]. The tolerance is ± 0.1 %.

The measurements made by spectrophotometry or cavity ring-down take into account the scattering, which increases rapidly as the wavelength of the light is decreased. But this has no effect on the distortion, the depolarization, the self-focusing or the laser damage. For high-power lasers, the thermal absorption coefficient must be known. For that purpose, we are going to limit our attention at 355 nm, the wavelength of our laser. This wavelength corresponds to a third harmonic of a YAG laser. Its repetition rate is 50 Hz. The P.D. is performed with a YAG laser [33] to measure materials and thin layers at 355 nm. The sensitivity of the method depends on the energy in the pulses, the overlap length between the probe and the pump beam and the spot size on the position sensor. The P.D. measures a deflection that is mainly due to the relative temperature coefficient but also to the thermal stress and expansion.
In this paper, the methods, the experimental setup, and the thermal program which has been developed to calculate deflections are described. The value from a BK7 sample will use as the absorption reference. The results on thin layers and silica sample are given from a BK7 sample.

2. Materials for photothermal deflection

The four measured samples were 50 mm in diameter and 5 mm in thickness. Two uncoated samples were made of BK7 and of silica. The BK7 sample was used for calibration. The other two were samples made of silica and coated by sol-gel process [34-39]. A bare silica sample was used to determine the absorption of the uncoated silica sample BK7 sample was used for calibration. The other two were coated samples by sol-gel process [34-39]. A bare silica sample was used to determine the absorption of the only silica sample .As these coated samples were manufactured by dip-coating [32], both faces of the sample were coated at the same time and the layers had the same thickness. Each face had a layer of 210 nm in thickness according to our analysis made from a transmission spectrum and a homemade program [43]. One of these two samples was post-processed to harden the sol-gel layer in order to make the layers more handleable. This process is called ammonia curing [41-43].
Table 1 gives the values of physical properties which are necessary to compute the Optical Path Difference (OPD) induced by the heating that was caused by the laser passing through the sample.

Table 1: Values of physical properties of BK7 [32] and silica [44].

Material	n	β [l0$^{-6}\cdot$K^{-1}]	α [10$^{-6}\cdot$K^{-1}]	λ_c [W$\cdot$m$^{-1}\cdot$K^{-1}]	E (N$\cdot$mm^{-2})	ν	γ [10$^{-6}\cdot$K^{-1}]
BK7	1.5151	1.35	7.1	1.114	81000	0.208	5
SiO_2	1.4570	9.8	0.51	1.38	73000	0.17	10

where:

n: is the refractive index of the material at 633 nm.

$\beta = \left[\frac{\partial n}{\partial T}\right]_{Absolute}$ is the relative temperature coefficient in the range [20-40°C].

α is the mean linear expansion coefficient in the range [-30 et 70°C].

λ_c is the heat conductivity.

E is the Young's modulus.

ν is the Poison's ratio.

$\gamma = (n\text{-}l)\cdot\alpha + \beta$.

3. Setup to measure absorption by photothermal deflection

Mistral bench was used to measure absorption at 355 nm. This bench had been used as a laser damage bench and it was clearly described in a previous paper [33]. Its setup is drawn in **Fig.5**.

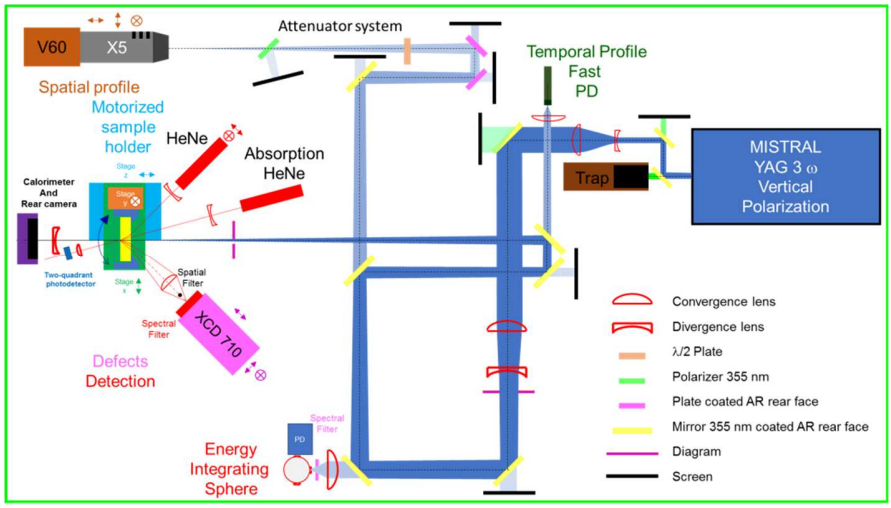

Fig. 5: Setup to measure absorption at 355 nm using a YAG laser working at 3ω (351 nm) [33].

The principle to measure the absorption is the longitudinal photothermal deflection which is illustrated by **Fig.6**.

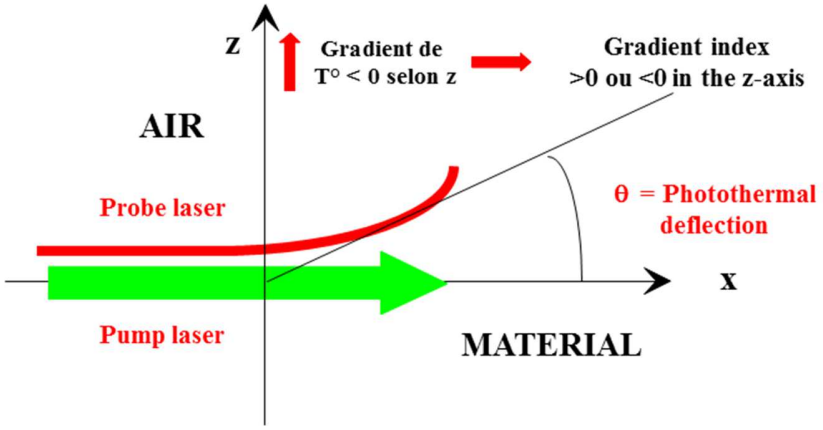

Fig. 6: Principle of longitudinal photothermal effect.

The pump beam came from Mistral which was a YAG working at 50Hz. The probe beam was a HeNe laser which was set at 30° incidence to the normal line. This laser was expended by a divergence lens in order to include the irradiated volume of matter by the pump laser. After the sample, a lens was put to focus the beam on a two quadrant detector, so the angular sensitivity was increased. The heating caused by the laser and the material absorption induced a temperature rise and so a gradient index. This gradient index deflected the probe beam and the laser spot on the two quadrant detector was translated. Before carrying out measurements, the sensor was set in translation and in rotation to equalize both voltages coming from each quadrant of the sensor. A lock-in amplifier was employed to detect small deflections; the reference signal being given by the synchronization signal of the laser. All the devices (laser, lock-in amplifiers, voltmeter …) were driven by a computer via an IEEE connection and LabView software. LabView is also used to save at the same time the results and the parameters of the device.

The heating of the material by the laser beam produces variations of refractive indexes and changes of lengths. If the OPD evolves, the P.D. also evolves. This method is more sensitive than the transverse photothermal deflection, but harder to calibrate because there is not a standard. The Δ = IJ = OPD change can be linked to photothermal deflection γ = P.D. by **Equation 1** (see **Fig.7**):

$$\gamma = \frac{4 \cdot \Delta}{D} \quad (1)$$

where D is the beam diameter.

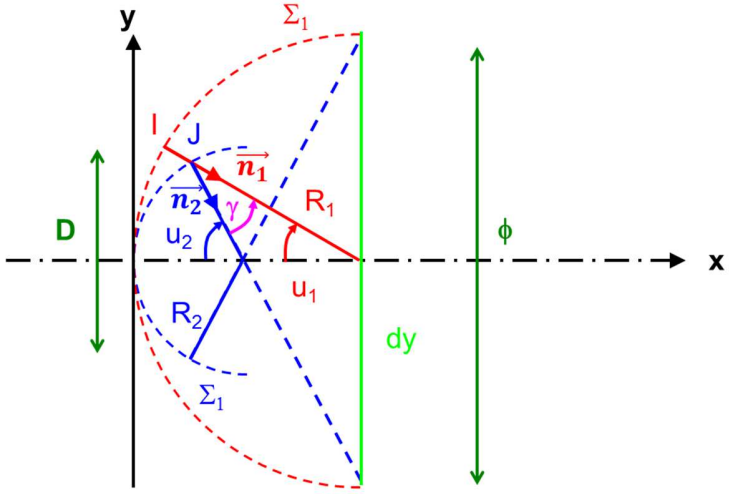

Fig. 7: Connection between IJ, the OPD and γ the ray deflection, for a beam having D as diameter.

4. Absorption measurement and numerical simulation.

4.1 Description of phenomenon

A power laser beam with a power P_0 and a radius r_1, is weakly absorbed by the material, according to the Beer Lambert's law, when it passes through a window or a rod with thickness t and absorption coefficient A. This absorption coefficient consisted of a thermal part A_T and a scattering part A_S which is presumed negligible ($A = A_T + A_S \approx A_T$). The absorbed power is given by **Equation 2**:

$$P_0 \cdot (1 - \exp(-A_T \cdot t)) \approx P_0 \cdot A_T \cdot t \quad (2)$$

This absorbed power induces a local temperature gradient $\frac{\partial T(r)}{\partial r}$ which produces a refractive index variation $\frac{\partial n(r)}{\partial r}$ and a mechanical expansion of the window as well as a thickness increase and so a stress increase $\frac{\partial \sigma(r)}{\partial r}$. This stress change leads to index modification $\frac{\partial n(r)}{\partial \sigma}$. All these variations yield variations of the P.D. The calculation can be found in the works coming from Claude Klein [45-46]. This P.D. is measured with a two quadrant detector [47-48].

4.2 Temperature calculation

The laser beam and the sample are assumed to have a cylindrical symmetry and the beam profile is a top hat of radius r_1 governed by **Equation 3** (cf. **Fig.8**).

$$\begin{cases} r \le r_1 & P(r) = \dfrac{P_0}{\pi \cdot r_1^2} \displaystyle\int_0^r 2 \cdot \pi \cdot u \cdot du = \left(\frac{r}{r_1}\right)^2 \cdot P_0 \\ r > r_1 & P(r) = \dfrac{P_0}{\pi \cdot r_1^2} \displaystyle\int_0^{r_1} 2 \cdot \pi \cdot u \cdot du = P_0 \end{cases} \quad (3)$$

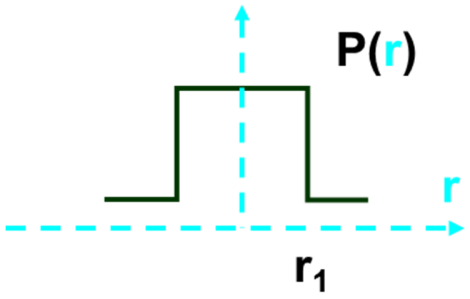

Fig. 8: Spatial profile of a uniform beam having a power P_0 and a radius r_1, P(r) is the integrated power.

Figure 9 is a diagram of material which is heated with a laser having a power P_0. This sample has a radius R, a length t, an absorption coefficient A_T (here the scattering is ignored $A = A_T + A_S = A_T$). The material is assumed optically transparent which means that the infrared radiations coming from heating are neglected. As the material is weakly absorbent, P_0 is constant along the z-axis and the absorbed flux in z is $A_T \cdot P_0 \cdot z$.

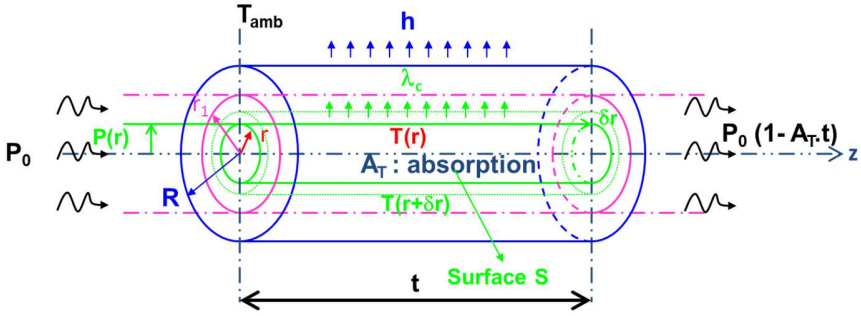

Fig. 9: Diagram of a material heated by laser absorption at room temperature.

The heat flux generated by absorption radially flows out to the periphery by conductivity and conducto-radiative heat transfer at the surface S. It also flows at both ends of the sample. This heat transfer to the surrounding environment is characterized with a generalized thermal coefficient h.

If the medium was assumed infinite with a cylindrical symmetry, the thermal balance is given by **Equation 4**:

$$\varphi_{Abs} = \varphi_{Cond} \quad \textbf{(4)}$$

where φ_{Abs} is the absorbed flux and φ_{Cond} is the conductive flux.

In our case, **Equation 4** yields a system of two equations according to r (**Equation 5**):

$$\begin{cases} r \le r_l & \varphi_{Abs} = \dfrac{A_T \cdot P_0}{\pi \cdot r_l^2} \cdot t \cdot \int_0^r 2 \cdot \pi \cdot u \cdot du = \left(\dfrac{r}{r_l}\right)^2 \cdot A_T \cdot t \cdot P_0 = \varphi_{Cond} = -2 \cdot \pi \cdot \lambda_c \cdot r \cdot t \cdot \dfrac{\partial T(r)}{\partial r} \\ r > r_l & \varphi_{Abs} = A_T \cdot t \cdot P_0 = \varphi_{Cond} = -2 \cdot \pi \cdot \lambda_c \cdot r \cdot t \cdot \dfrac{\partial T(r)}{\partial r} \end{cases} \quad (5)$$

The analytical solutions of this system are given by **Equation 6**:

$$\begin{cases} r \le r_l & \partial T_1(r) = -\dfrac{A_T.P_0}{2.\pi.\lambda_c}.\left(\dfrac{r}{r_l^2}\right).\partial r & \Rightarrow & T_1(r) = T_0 - \dfrac{A_T.P_0}{2.\pi.\lambda_c}.\dfrac{1}{2}\left(\dfrac{r}{r_l}\right)^2 \\ r > r_l & \partial T_1(r) = -\dfrac{A_T.P_0}{2.\pi.\lambda_c}.\dfrac{\partial r}{r} & \Rightarrow & T_2(r) = C - \dfrac{A_T.P_0}{2.\pi.\lambda_c}.\mathrm{Log}(r) \\ \text{With} & T_1(r_l) = T_2(r_l) & \Rightarrow & C = T_0 - \dfrac{A_T.P_0}{2.\pi.\lambda}\left[\dfrac{1}{2} - \mathrm{Log}(r_l)\right] \\ \text{so } r \le r_l & T_1(r) = T_0 - \dfrac{A_T.P_0}{2.\pi.\lambda_c}.\dfrac{1}{2}\left(\dfrac{r}{r_l}\right) & \Rightarrow & \Delta T_1(r) = \dfrac{A_T.P_0}{2.\pi.\lambda_c}.\dfrac{1}{2}\left(\dfrac{r}{r_l}\right)^2 \\ r > r_l & T_2(r) = T_0 - \dfrac{A_T.P_0}{2.\pi.\lambda_c}.\left[\dfrac{1}{2} + \mathrm{Log}\left(\dfrac{r}{r_l}\right)\right] & \Rightarrow & \Delta T_2(r) = \dfrac{A_T.P_0}{2.\pi.\lambda_c}.\left[\dfrac{1}{2} + \mathrm{Log}\left(\dfrac{r}{r_l}\right)\right] \end{cases} \quad (6)$$

Figure 10 shows the radial profile of the difference in temperature of a BK7 sample having 8 mm in thickness, 76 mm in diameter and A_T = 0.27 m^{-1} in absorption coefficient irradiated with a uniform laser beam of 1 mm in radius with two powers 10 and 100 W. In the insert, for the same configuration, the maximum difference in temperature is plotted according to the laser power.

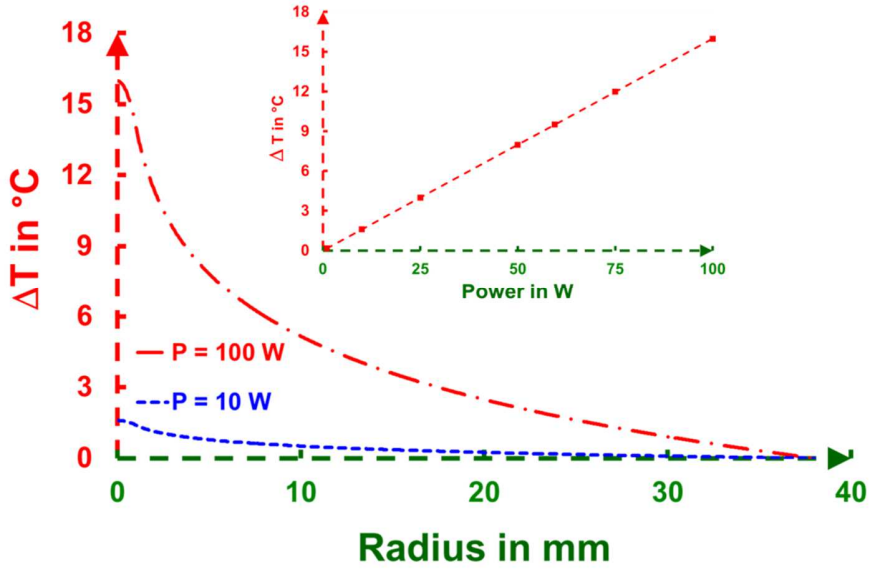

Fig. 10: Radial profile of temperature of a 8 mm in thickness and 76 mm in diameter substrate made of BK7 having an absorption coefficient A_T = 0.27 m^{-1} heated with a laser of 10 and 100 W of power with a uniform intensity profile on a 1 mm in radius. In the inset, the difference of

the temperature between the center and the edge for several incidence laser powers is drawn.

The slope of this curve is $\frac{A_T}{4 \cdot \pi \cdot \lambda_c}$.

If boundary conditions are taken into account at a periphery and at both ends, the thermal equilibrium is given by **Equation 7**:

$$\varphi_{Abs} = \varphi_{Conductive} + \varphi_{Convective} + \varphi_{Radiative} = \varphi_{Conductive} + \varphi_{Conv\text{-}Rad} \quad (7)$$

The expressions of the different fluxes are given in **Equation 8**:

$$\begin{aligned} \varphi_{Absorbed}(r) &= 2 \cdot \pi \cdot A_T \cdot t \cdot \int_{u=0}^{u=r} P(u) \cdot u \cdot du \\ \varphi_{Conductive}(r) &= -2.\pi.r.\lambda.t.\frac{\partial T(r)}{\partial r} \\ \varphi_{Convective}(r) &= 2 \cdot \left(2 \cdot \pi \cdot h_c \cdot \int_{u=0}^{u=r} \left[T(u) - T_{Ambient} \right] \cdot u \cdot du \right) \\ \varphi_{Radiative}(r) &= 2 \cdot \left(2 \cdot \pi \cdot \varepsilon \cdot \sigma \cdot \int_{u=0}^{u=r} \left[T(u)^4 - T_{Ambient}{}^4 \right] \cdot u \cdot du \right) \end{aligned} \quad (8)$$

where h_c is the convective heat transfer coefficient,

ε_{IR} is the material emissivity,

$\sigma_{Stephan}$ is the Stephan's constant $\sigma = 5.670373 \cdot 10^{-8}\ W \cdot m^{-2} \cdot K^{-4}$,

t is the sample thickness.

Since the material is weakly absorbent, the temperature increase is weak and T(u) is close to $T_{Ambient} = 293$ K. The wavelength peak from infrared emission is around 10 µm according to Wien's law. The material is nearly in the same thermal emission regime. The silica and the BK7 are completely opaque after 5 µm. Both of these materials have an emissivity $\varepsilon_{IR} = 1$ according to the Kirchhoff's law. Within this temperature range, this law can be linearized (**Equation 9**). Over the range [293-313 K], the error remains lower than 10%.

$$\sigma_{Stephan} \cdot (T(u)^4 - T_{Ambient}{}^4) = 4 \cdot \sigma_{Stephan} \cdot T_{Ambient}{}^3 \cdot \Delta T(u) = h_R \cdot \Delta T(u) \quad (9)$$

For $T_{Ambient} = 293$ K, the radiative transfer coefficient h_R is equal to 5.71 $W \cdot m^{-2} \cdot K^{-1}$. So, the convective and radiative terms can be added and the corresponding flux replaced by a convecto-radiative flux having a transfer coefficient $h = h_c + h_R$. The convective heat transfer coefficient h_c is taken equal to 5 $W \cdot m^{-2}$ within our temperature range.

The thermal equilibrium equation is now given by **Equation 10**:

$$2 \cdot \pi \cdot A_T \cdot t \cdot \int_{u=0}^{u=r} P(u) \cdot u \cdot du = -2 \cdot \pi \cdot r \cdot \lambda_c \cdot t \cdot \frac{\partial T(r)}{\partial r} + 4 \cdot \pi \cdot h \cdot \int_{u=0}^{u=r} \Delta T(u) \cdot u \cdot du \quad (10)$$

with the boundary conditions:

At both cylinder ends z = 0 and z = t

$$\left[\frac{\partial T(r)}{\partial r}\right]_{z=0 \text{ and } z=t} = \left[\frac{\partial \Delta T(r)}{\partial r}\right]_{z=0 \text{ and } z=t}$$

At r = R, the flux emitted by the cylinder is equal to the absorbed flux

$$2\cdot\pi\cdot e\cdot h\cdot T\cdot\Delta T(R)+4\cdot\pi\cdot h\cdot\int_{u=0}^{u=r}\Delta T(u)\cdot u\cdot du = 2\cdot\pi\cdot A_T\cdot t\cdot\int_{u=0}^{u=r}P(u)\cdot u\cdot du$$

The periphery Both ends Absorbed flux

Continuous flux at r = R $\forall z$

$$-\lambda_c\cdot\left[\frac{\partial T(r)}{\partial r}\right]_{r=R,\ \forall z}$$

These equations can be solved numerically for example using Mathematica.

4.3 Introduction of stresses and OPD linked to temperature evolution

The absorption of a power laser beam by a material induces modifications of its shape and of its refractive index. The variation of the OPD Δ = t (n-1) along the propagation direction z according to the temperature T is given by **Equation 11** [45-46, 49]:

$$\delta\Delta = (n-1)\cdot\delta t + t\cdot\delta n$$

$$\delta t = (\alpha+\varepsilon_z)\cdot t \quad \text{and} \quad \delta n = (\delta n)_T + (\delta n)_{Stress} = \left[\frac{\partial n}{\partial T}\right]_{\Delta\sigma=0}\cdot\delta T + \left[\frac{\partial n}{\partial \sigma}\right]_{\Delta T=0}\cdot\delta\sigma \qquad (11)$$

$$\varepsilon_z = \begin{cases} \alpha\cdot\delta T - \dfrac{\upsilon}{E}\cdot(\sigma_r+\sigma_\theta) & \text{if the window is thin} \\ \alpha\cdot\delta T + \dfrac{1}{E}\cdot(\sigma_z - \upsilon\cdot(\sigma_r+\sigma_\theta)) & \text{if the window is thick} \end{cases}$$

where

$\left[\frac{\partial n}{\partial T}\right]_{\Delta\sigma=0} = \beta$ is the relative temperature coefficient.

$\left[\frac{\partial n}{\partial \sigma}\right]_{\Delta T=0} = K$ is the photo-elastic coefficient [50].

ε_z is the strain component along z.

σ is the stress tensor.

σ_r, σ_θ, σ_z are the radial, orthoradial and longitudinal stresses.

The window is thin if its diameter is higher than its thickness either it is thick, it is a rod.

The expression of $\delta\Delta$ (**Equation 12** and **13**) for both cases are given in previous papers [45-46, 51] for an isotropic medium:

Thin window:

$$\delta\Delta(r) = t.\left(\beta+(n-1).\alpha.(1+\upsilon)+\frac{n^3.\alpha.E}{4}.(q_{\square}+q_{\perp})\right).\delta T(r) \qquad (12)$$

Thick window:

$$\delta\Delta(r) = t \cdot \left(\beta + \frac{n^3 \cdot \alpha \cdot E}{4 \cdot (1+\upsilon)} \cdot \left(q_{\parallel} + 3 \cdot q_{\perp} \right) \right) \cdot \delta T(r) \quad (13)$$

where

$q_{//}$ is the piezo-optic coefficient for parallel polarization.

$q_{\perp}$ is the piezo-optic coefficient for perpendicular coefficient.

The equations between the piezo-optic coefficients $q_{//}$, $q_{\perp}$ and the photo-elastic coefficients $K_{//}$, $K_{\perp}$ are established in previous papers [45, 51] and are given by **Equation 14**. Their values are summarized in **Table 2**.

$$K_{\parallel} = \frac{\partial n}{\partial \sigma_r} = -\frac{n^3}{2} \cdot q_{\parallel} \quad \text{and} \quad K_{\perp} = \frac{\partial n}{\partial \sigma_\theta} = -\frac{n^3}{2} \cdot q_{\perp} \quad (14)$$

Table 2: Values of $K_{//}$ and $K_{\perp}$ for BK7 and silica [50, 52].

Material	$K_{//}$ (Pa^{-1})	$K_{\perp}$ (Pa^{-1})	$K = K_{//} - K_{\perp}$ (Pa^{-1})
BK7	$-0.5 \cdot 10^{-6}$	$-3.37 \cdot 10^{-6}$	$2.85 \cdot 10^{-6}$
SiO_2	$-0.62 \cdot 10^{-6}$	$-4.34 \cdot 10^{-6}$	$3.72 \cdot 10^{6}$

Some examples of analytical (A) and numerical (N) calculations for silica and BK7 samples having similar sizes (76 mm in diameter and 8 mm in thickness) and absorption coefficient ($A_T = 0.27$) are plotted in **Fig.11** for a laser beam of 100 W power with a uniform profile and 1 mm in radius of waist. In these cases, the transfer coefficient is 10.71 $W \cdot m^{-2}$ and the room temperature is 293 K

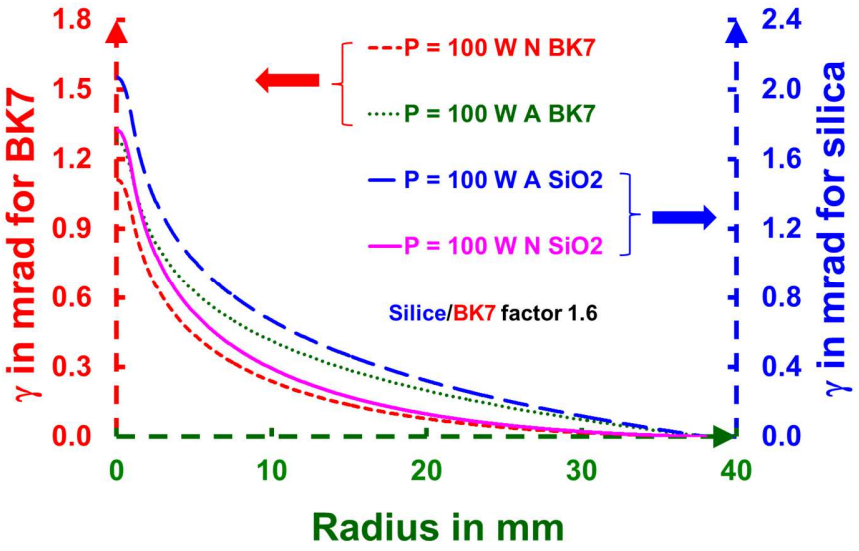

Fig. 11: Analytical and numerical calculations of the photothermal deflection γ as a function of radius r with a laser beam of 100 W power and 1 mm in radius (uniform profile) for same thickness, same diameter and same absorption coefficient (0.27 m^{-1}) samples made of BK7 and silica. The transfer coefficient h = 10.71 $W \cdot m^{-2}$ and the surrounding environment temperature $T_{ambient}$ = 293K.

Figure 11 shows that for similar irradiation parameters of a laser beam, the photothermal deflection is 1.6 times larger for silica than for BK7 glass.

To have the absorption coefficient A_T a fit between the measurement and the analytical model is made to get a first value from **Equation 15**:

$$\Delta(r) = A_T \cdot P \cdot \frac{\gamma \cdot t}{2 \cdot \pi \cdot \lambda} \cdot f(r) \quad \text{with} \quad \gamma = (n-1) \cdot \alpha + \beta$$

$$f(r) = \begin{cases} \frac{1}{2} \cdot \left(\frac{r}{r_l} \right)^2 & \text{if } r < r_l \\ \frac{1}{2} + \text{Log}\left(\frac{r}{r_l} \right) & \text{if } r_l < r < R \end{cases} \qquad \text{hence} \quad A_T = \frac{\int_0^R \Delta(r) \cdot dr}{P \cdot \frac{\gamma \cdot t}{2 \cdot \pi \cdot \lambda} \cdot \int_0^R f(r) \cdot dr} \qquad (15)$$

A complete calculation of the wavefront distortion [45-46] will be achieved from this first value to optimize it by taking into account the thermal losses by radiation and convection and photo-elastic coefficients.

5. Results and discussion

The difference in the temperature ΔT and the OPD Δ of BK7 and silica samples having the same absorption coefficient $A_T = 0.27$ has been computed thanks to our models above and drawn in **Fig 12** and **13**. The results are inferior for the digital computing than for the analogical one because the convective flux and the radiative flux cooled the samples. As the thermal conductivity of silica is higher than the one of BK7, the reached temperature is lower in silica than in BK7.

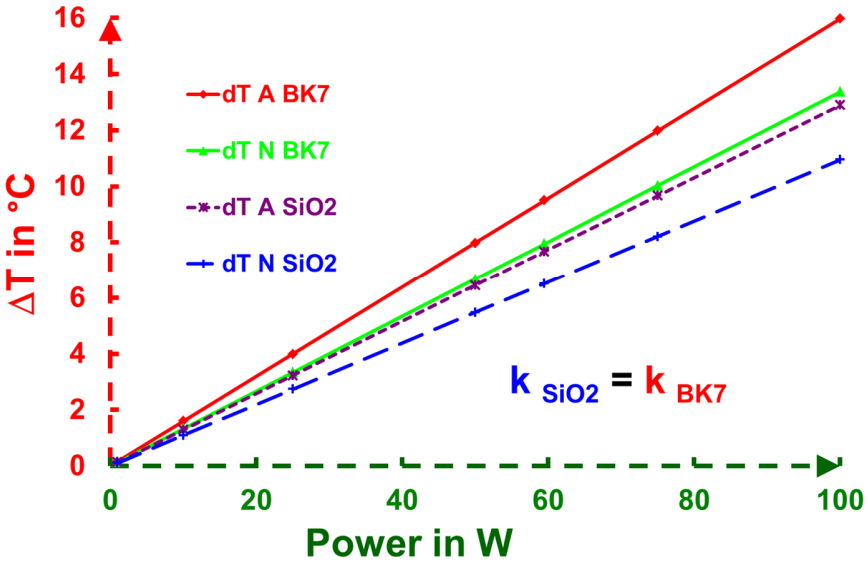

Fig. 12: ΔT between silica and BK7 as a function of the laser power.

Although the reached temperatures in the silica are less than in the BK7, the parameter γ of silica is higher than BK7, involves a higher OPD for silica than for BK7. For the same parameters of sample and laser beam, the OPD is 1.6-fold higher for silica than for BK7 glass as illustrated in **Fig.13**.

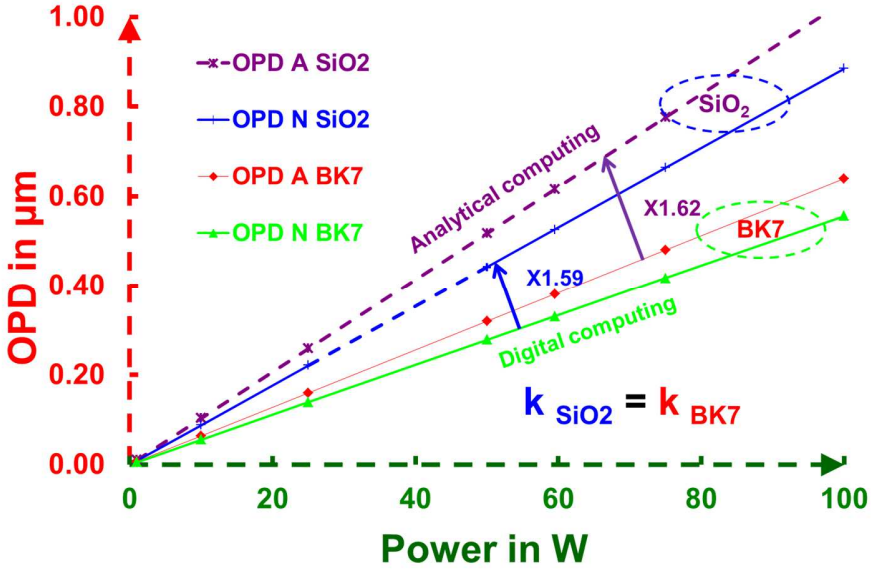

Fig. 13: OPD between silica and BK7 as a function of laser power.

The four samples described in paragraph 2.2 have been measured with a Mistral apparatus as a function of energy per pulse. The results are plotted in **Fig.14** and presented in **Table 3**.

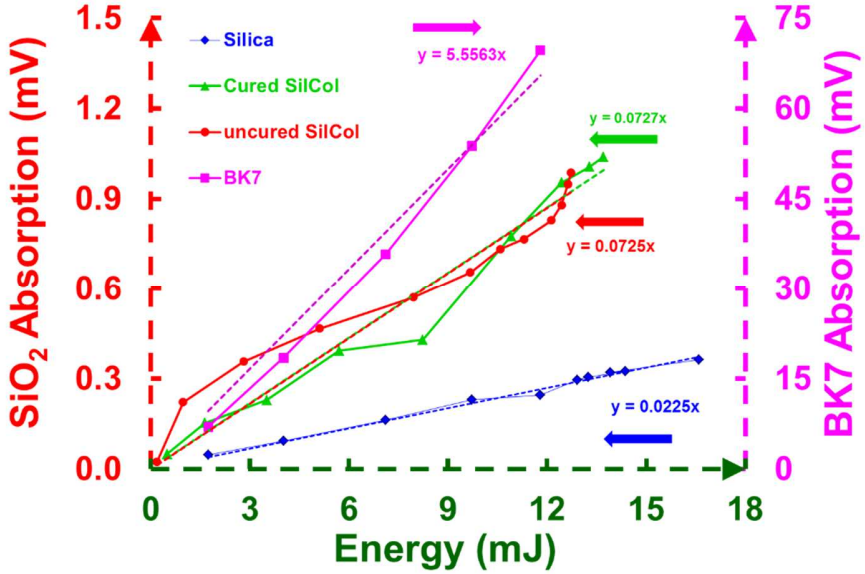

Fig. 14: Experimental results of absorption measurement for different samples in a.u. as a function of the laser power.

Table 3: Slopes coming from experimental absorption measurements of several sample (cf. Fig.14).

Sample	BK7	Bare Silica	Uncured Silcol	Cured Silcol
Slope y ($V \cdot J^{-1}$)	5.556	0.0225	0.0725	0.0727

As here the photothermal deflection linearly depends on the absorbed power in this fluence range, the silica is less absorbent than the BK7. In addition, according to **Fig.13** a same absorption gives an OPD and a P.D. 1.6 times higher for silica than for BK7. A P.D. must be added if the sample, having a thickness t, is traversed by a probe laser at 633 nm under 30° incidence angle because $l \neq t$ (see **Fig. 15**).

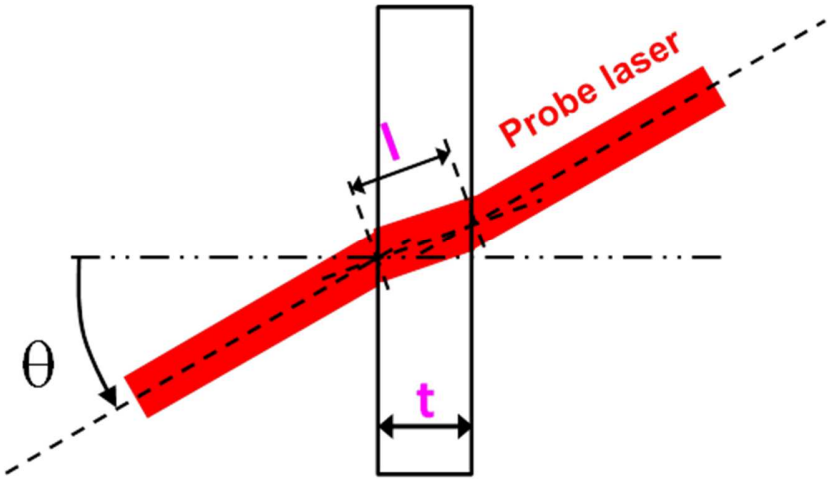

Fig. 15: Diagram showing the OPD for a flat sample of thickness t linked to incidence angle θ.

To evaluate the silica absorption, Equation 16 is used:

$$A_{355\ nm\ SiO_2} = \frac{Slope_{SiO_2}}{Slope_{BK7}} \cdot \frac{1}{coeff_D} \cdot A_{355\ nm\ BK7}$$

$$A_{355\ nm\ SiO_2} = \alpha_{355\ nm\ SiO_2} \cdot l_{SiO_2}$$

$$A_{355\ nm\ BK7} = \alpha_{355\ nm\ BK7} \cdot l_{BK7} \qquad (16)$$

$$l_{SiO_2\ or\ BK7} = \frac{t}{\cos\left[\mathrm{Arc}\sin\left(\frac{\sin\theta_{Probe}}{n_{SiO_2\ or\ BK7\ at\ 633\ nm}}\right)\right]}$$

As the datum for absorption coefficient is $\alpha_{355\ nm\ BK7} = 2.596\ m^{-1}$ [32] the numerical application gives for silica, $\alpha_{355\ nm\ SiO2} = 6.47 \cdot 10^{-3}\ m^{-1}$, so an attenuation of 28 $dB \cdot km^{-1}$. These values are compatible with the 50-70 $dB \cdot km^{-1}$ which can be estimated from **Fig.2** because this silica contains few OH^- ions The absorptions of cured and uncured layers of silcol are given by **Equation 17**:

$$A_{355\ nm\ Silcol\ cured\ or\ uncured} = \frac{Slope_{Silcol\ cured\ or\ uncured}}{Slope_{BK7}} \cdot \frac{1}{coeff_D} \cdot A_{355\ nm\ BK7} \qquad (17)$$

The absorptions are of 111 ppm for an uncured layer and of 114 ppm for a cured layer. These absorptions match the silica substrate absorption (34 ppm) and the absorption of both deposited layers by dip-coating technique. As a result, the absorptions of an uncured silcol layer and a cured silcol layer are similar: $A_{T\ Uncured\ Silcol} = 38\ ppm = A_{T\ Cured\ Silcol}$

As the measured layers have a 210 nm in thickness in order to be almost antireflective coatings at 1053 nm, the extinction coefficients k can be evaluated by **Equation 18**:

$$k_{T\ 355\ nm\ Silcol\ cured\ or\ uncured} = \frac{A_{Silcol\ cured\ or\ uncured}}{4 \cdot \pi} \cdot \frac{\lambda}{l_{Silcol\ cured\ or\ uncured}}$$

where

$$l_{Silcol\ cured\ or\ uncured} = \frac{t_{Silcol\ cured\ or\ uncured}}{\cos\left[\mathrm{Arc}\sin\left(\frac{\sin\theta_{Probe}}{n_{Silcol\ at\ 633\ nm}}\right)\right]} = 222\ \mathrm{nm} \qquad (18)$$

Because $n_{Silcol\ at\ 633\ nm} = 1.22$

So $k_{T\ 355\ nm\ Uncured\ Silcol} = k_{T\ 355\ nm\ Cured\ Silcol} = 4.8 \cdot 10^{-6}$. These extinction coefficients of thermal origin are clearly less (1000 factor) than the extinction coefficients found by spectrophotometry, which came mainly from the scattering of these layers linked to their crazing [43].

All the results of absorption measurements are summarized in **Table 4**.

Table 4: Summary of the absorption measurements of our four samples.

Material	BK7	Bare Silica	Uncured Silcol	Cured Silcol
Refractive index	1.515	1.457	1.22	1.22
Slope y (V/J)	5.556	0.0225	0.0725	0.0727
α_{355} nm (m^{-1})*	2.596	0.00647		
l(mm)	5.297	5.323	5.323	5.323
Absorption (ppm)	13748	34	38	38
k_T (355 nm)	$7.33 \cdot 10^{-8}$	$1.8 \cdot 10^{-10}$	$4.8 \cdot 10^{-6}$	$4.8 \cdot 10^{-6}$

*$\alpha_{355\ nm}$ corresponds to the whole sample (bulk and layers if coatings)

The extinction coefficient at 355 nm of silica is very low; it is 400 times lower than of BK7. At 355 nm, the silica attenuation is 28 $dB \cdot km^{-1}$. Sometimes it is necessary to take into account silica absorption to estimate absorption of thin films and their extinction coefficients. The values founded for silica layers made by sol-gel remain coherent with this process of deposition.

6. Conclusion

The thermal deflection is employed to measure the absorption of bulk material and sol-gel layers by using the longitudinal effect. With this technique, the probe and pump beams are not perfectly collinear. The setup has been presented. It uses a pump laser with a low rate repetition (YAG) which has been used to measure the laser damage threshold. To help the interpretation of measurements, a program has been implemented with an analogic part and a digital part. The analogic part has been applied to fit our interferometric measurement to get a first value of an absorption coefficient. The digital part takes into account the thermal losses caused by radiative and convective fluxes which is beneficial to obtain a lower temperature.. The temperature rises of the material linked to the heating laser, induce also stresses which modify the P.D. These stresses are also taken into account by our code. Thanks to theoretical and experimental aspects, the absorptions of weakly absorbent materials have been measured like for silica, BK7 and sol-gel layers at 355 nm. The values from BK7 have been used to calibrate the photothermal experience with our code. This code shows that for a same absorption in BK7 and in silica, the effects on the wavefront are 1.6 times higher on silica

than on BK7. The energy per pulse does not lead to non-linear effect, thus the absorption remains linear and the absorption coefficients can be evaluated. From these ones and the configuration of measurements, it makes it possible to evaluation the extinction coefficient of the material or of the layer. So, the attenuation of silica at 355 nm has been found to be equal to 28 $dB \cdot km^{-1}$. In the cases of thin films made by dip-coating, the extinction coefficients of these films are close to $5 \cdot 10^{-6}$. The ammoniac curing carried out to harden the sol-gel layer does not influence on the absorption of sol-gel layers. This method is applicable for all materials which are weakly absorbent if all parameters (n, λ, β, α , ν…) are known and if we are in the linearity field of the 4 quadrant detectors.

Acknowledgements

J. Avice was thanked for the manufacture of sol-gel coatings used in order to write this paper.

References

1. C. Zhao, J. Degallaix, L. Ju, Y. Fan, D.G. Blair, B.J.J. Slagmolen, M.B. Gray,C.M. Mow Lowry, D.E. McClelland, D.J. Hosken, D. Mudge, A. Brooks, J. Munch,p. J. Veitch, M.A. Barton, G. Billingsley, "Compensation of strong thermal lensing in high optical-power cavities," Phys. Rev. Lett. **96,** 231101.(2006)
2. W. Winkler, K. Danzmann, A. Rdiger, R. Schilling, "Heating by optical absorption and the performance of interferometric gravitational-wave detectors," Phys. Rev. A **44,** 7022-7036 (1991).
3. Y. Peng, Z. Sheng, H. Zhang, X. Fan, "Influence of thermal deformations of the output windows of high-power laser systems on beam characteristics," Appl.Opt. **43**, 6465- 6472 (2004)
4. E. Ohmura "Analyses of Self-Focusing Phenomenon and Temperature Rise in Fused Silica by Ultrashort Pulse Laser Irradiation," Procedia CIRP, **5**, 7-12 (2013)
5. O. M. Efimov "Self-focusing of tightly focused laser beams," App. Opt. **54** (22), 6895-6903 (2015)
6. U. Neukirch, D. C. Allan, N. F. Borrelli, C. E. Heckle, M. M., J. Moll, C. M. Smith, "Laser-induced birefringence in fused silica from polarized lasers," Proc. SPIE **5754,** 637-645 (2004)
7. B. McMillen, Y. Bellouard, "On the anisotropy of stress-distribution induced in glasses and crystals by non-ablative femtosecond laser exposure," Opt Express **23**(1):86-100 (2015)
8. L.B. Glebov, "Intrinsic laser-induced breakdown of silicate glasses," Proc. SPIE **4679,** 321-331 (2002).
9. M. Pawlak, M.Chirtoc, N.Horny, J.Pelzl,"Spectrally Resolved Modulated Infrared Radiometry (SR-MIRR) of Photothermal, Photocarrier and Photoluminescence Response of CdSe Crystals: Determination of Optical, Thermal and Electronic Transport Parameters," J. Appl. Phys. **119**, 125108(2016).
10. M. Pawlak, S. Pal, A.Ludwig, A.D.Wieck,"On the infrared absorption coefficient measurement of thick heavily Zn doped GaAs using spectrally resolved modulated photothermal infrared radiometry," J. Appl. Phys. **122** 135109 (2017).
11. " Concepts of optical fiber communication" https://www.slideshare.net/naveenjakhar12/concepts-of-optical-fiber-communication-65963761
12. "FOP Series Fibre Optic Bundles" https://www.bentham.co.uk/products/components/components-search/fop-series-fibre-optic-bundles-10/#measurement/ (https://www.bentham.co.uk/products/components/components-search/fop-series-fibre-optic-bundles-10/#measurement/)
13. D.B Keck, R.D Maurer, P.C. Schultz. "On the ultimate lower limit of attenuation in glass optical waveguides." Appl. Phys. Lett.**,** ***22*** (7), 307-309 (1973).
14. V. Loriette, C. Boccara, "Absorption of low-loss optical materials measured at 1064 nm by a position-modulated collinear photothermal detection technique," App. Opt. **42** (4), 649-656 (2003).
15. https://www.heraeus.com/en/hqs/fused_silica_quartz_knowledge_base/t_calc/transmission_calculator.aspx
16. P. Voarino, H. Piombini, F. Sabary, D. Marteau, J. Dubard, J. Hameury,J. R. Filtz, " High-accuracy measurements of the normal specular reflectance," App. Opt. **47**(13), C303-C309 (2008).
17. J. M. Herbelin, J. A. McKay, M. A. Kwok, R. H. Ueunten, D. S. Urevig, D. J. Spencer, and D. J. Benard, " Sensitive measurement of photon lifetime and true reflectances in an optical cavity by a phase-shift method," App Opt. **19** (1), 144-147 (1980).
18. A. O'Keefe and D. A. G. Deacon, "Cavity ring-down optical spectrometer for absorption measurements using pulsed laser sources,"Rev. Sci. Instrum. **59,** 2544–2551 (1988).
19. K. V. Vlasova, A. I Makarov, N. F. Andreev, A. Yu. Konstantinov "High-sensitive absorption measurement in transparent isotropic dielectrics with time-resolved photothermal common-path interferometry," App. Opt. **57**(22), 6318 (2018).
20. W. Triebel, C. Mühlig, S. Kufert, "Application of the laser-induced deflection (LID) technique for low absorption measurement in bulk materials and coatings," Proc. SPIE **5965**, 59651J (2005).
21. B. Cimma; D. Forest; P. Ganau; B. Lagrange; J. M. Mackowski; C. Michel; J. L. Montorio; N. Morgado; R. Pignard; L. Pinard; A. Remillieux, "Original optical metrologies of large components," Proc. SPIE **5252**, 332-334 (2004).
22. C. Mühlig, A. Bochmann, W. Triebel, and S. Kufert, "Laser-induced deflection (LID) technique for thermal lens evaluation and direct absorption measurements," Proc. SPIE **7132**, 71320R (2008).

23. C. Boccara, D. Fournier, W. Jackson, N.M. Amer, "Sensitive photothermal deflection technique for measuring absorption in optically thin media," Opt. Lett. **5** (9) pp 377-379 (1980).
24. P. Y. Baures and C. N. Man, "Measurements of optical absorption at 1.06 μm in low-loss materials," Opt. Mater. **2**, 241–247 (1993).
25. S. Yoshida, D.H. Reitze, D.B. Tanner,J. D. Mansell "Method for measuring small optical absorption coefficients with use of a Shack–Hartmann wave-front detector", App. Opt. **42** (24), 4835-4840 (2003).
26. S. Hild, H. Lück, W. Winkler, K.A. Strain, H. Grote, J.R. Smith, M. Malec, M. Hewitson, B. Willke, J. Hough, and K. Danzmann, "Measurement of a low-absorption sample of OH-reduced fused silica," Appl. Opt. **45** (28), 7269-72 (2006).
27. B. Schäfer, J. Gloger, U. Leinhos, K. Mann, "Photo-thermal measurement of absorptance losses, temperature induced wavefront deformation and compaction in DUV-optics;" Opt. Express **17** (25), 23025-230236 (2009).
28. H. Piombini; X. Dieudonné, T. Wood, F. Flory, "Guided wave measurements for characterization of sol-gel layers," Opt. Rev. **20** (5), pp.426-432 (2013).
29. M. Commandré; L. Bertrand; G. Albrand; E. Pelletier,"Measurement of Absorption Losses of Optical Thin Film Components by Photothermal Deflection Spectroscopy," Proc SPIE. **0805**,128-135(1987)
30. M. Commandré , E. Pelletie,r "Measurements of absorption losses in TiO2 films by a collinear photothermal deflection technique," App. Opt. **29 (28)**, 4276-4283(1990).
31. M. Commandré, P. Roche," Characterization of optical coatings by photothermal deflection," App. Opt. **35** (25), 5021-5034 (1996).
32. https://refractiveindex.info/?shelf=glass&book=BK7&page=SCHOTT
33. J. Avice, H. Piombini, C. Boscher, G. Vaudel, G. Brotons , P. Ruello ,V. Gusev,"Link between mechanical strength and laser damage threshold for antireflective coating made by sol-gel," Proc. SPIE **10447** (2017).
34. W. Stöber, F. Fink, E. Bohn, "Controlled growth of monodisperse silica spheres in the micron size range," J. Colloid Interface Sci. **26**(1), 62-69 (1968)
35. I. M. Thomas, "Method for the preparation of porous silica antireflection coatings varying in refractive index from 1.22 to 1.44," Appl. Opt., **31**, 6145 (1992).
36. D. Meyerhofer, "Characteristic of resist films produced by spinning", J. Appl. Phys. **49**, 3993 (1978).
37. L. E. Scriven, "Physics and applications of dip coating and spin coating", MRS proceedings **121** (1988).
38. C. J. Brinker, G. W. Scherer, Sol-Gel Science, "The Physics and Chemistry of Sol-Gel Processing, Academic Press, (1990).
39. C. J. Brinker, "Hydrolysis and condensation of silicates : Effects on structure",Non-Cryst. Solids., Vol. 100, pp. 31_50 (1988).
40. Landau, L. D.; Levich, V.G. Dragging of a liquid film by moving plate. Acta Physicochim. 1942, 17, 41
41. Belleville, P.; Floch, H. Ammonia hardening of porous silica antireflective coatings. SPIE Proc. **2288**, 25-32 (1994).
42. Avice, J.; Boscher, C.; Vaudel, G., Brotons, G.; Juvé, V.; Edely, M.; Méthivier, C.; Gusev, V. ; Belleville, P.; Piombini, H.; Ruello, P. Controlling the nanocontact nature and the mechanical properties of a silica nanoparticles assembly. J. Phys. Chim. **C 121**, 23769-23776 (2017).
43. Avice, J.; Boscher, C.; Voarino, P.; Brotons, G.; Piombini, H. Quantitative Estimation of Crazing in Sol-Gel Layers by Automated Optical Microscopy Analysis. Opt. Express **25** (23), 28851-28869 (2017).
44. Fused Silica, Corning code 7940" Calatog Corning Technical Products Division
45. C. A. Klein, "Optical distortion of high power laser windows," Opt. Eng., **29**(4), 343-350 (1990).
46. C. A. Klein "High-energy laser windows: case of fused silica," OE, **49** (9), 091006-1 091006-10(2010).
47. M. Pommiès, D. Damiani, X. Le Borgne, A. Surmin, J.-C. Birolleau, F. Pilon, C. Dujardin, B. Bertussi, H. Piombini, "Impurities detection by optical techniques in KH2PO4 crystals," Proc. SPIE **6403**, 8506-8516 (2007).
48. M. Pommiès, D. Damiani, B. Bertussi, J. Capoulade, H. Piombini, J.Y. Natoli, H. Mathis, "Detection and characterization of absorption heterogeneities in KH2PO4 crystals," Opt. Commun. **267**, 154–161(2006).
49. S. Timoshenko and J. N. Goodier, Theory of Elasticity (McGraw Hill, 1970).
50. "Variations des indices de réfraction des verres optiques par contraintes de compression et de traction" NT Ti n° 20 de chez Schott.
51. H. Piombini, F. Compoint, C. Ambard, D. Picart, P. Belleville, G. Damamme, F. Brémand,"Stress measurement of elastic sol-gel layer by photoelasticimetry - comparison with Stoney," OMEx **6** (2), 469-485 (2016).
52. C. A. Klein, "Toward an athermal HEL optical window: Is oxyfluoride glass the way to go?" Proc. SPIE 5991 59910S-1 (2005).